Optics Letters

Burst-mode thulium all-fiber laser delivering femtosecond pulses at a 1 GHz intra-burst repetition rate

Parviz Elahi,[1] Hamit Kalaycioğlu,[1,*] Önder Akçaalan,[1] Çağri Şenel,[2,3] and F. Ömer Ilday[1,4,5]

[1]Department, of Physics, Bilkent University, Ankara 06800, Turkey
[2]TÜBITAK National Metrology Institute (UME), PO54, TR-41470 Gebze, Kocaeli, Turkey
[3]Department of Physics, Boğaziçi University, 34342 Istanbul, Turkey
[4]Department of Electrical and Electronics Engineering, Bilkent University, Ankara 06800, Turkey
[5]UNAM-National Nanotechnology Research Center and Institute of Materials Science and Nanotechnology, Bilkent University, Ankara 06800, Turkey
*Corresponding author: hamitkal@bilkent.edu.tr

Received 23 June 2017; revised 18 August 2017; accepted 23 August 2017; posted 25 August 2017 (Doc. ID 300574); published 21 September 2017

We report on the development of, to the best of our knowledge, the first ultrafast burst-mode laser system operating at a central wavelength of approximately 2 μm, where water absorption and, consequently, the absorption of most biological tissue is very high. The laser comprises a harmonically mode-locked 1-GHz oscillator, which, in turn, seeds a fiber amplifier chain. The amplifier produces 500 ns long bursts containing 500 pulses with 1 GHz intra-burst and 50 kHz inter-burst repetition rates, respectively, at an average power of 1 W, corresponding to 40 nJ pulse and 20 μJ burst energies, respectively. The entire system is built in an all-fiber architecture and implements dispersion management such that output pulses are delivered directly from a single-mode fiber with a duration of 340 fs without requiring any external compression. This gigahertz-repetition-rate system is intended for ablation-cooled laser material removal in the 2 μm wavelength region, which is interesting for laser surgery due to the exceptionally high tissue absorption at this wavelength.

OCIS codes: (140.7090) Ultrafast lasers; (140.3280) Laser amplifiers; (060.3510) Lasers, fiber; (060.2320) Fiber optics amplifiers and oscillators.

https://doi.org/10.1364/OL.42.003808

Fiber lasers with all-fiber architecture, guiding light through optical fibers to the point of exit from the laser system, continue to attract attention as practical and robust sources for various applications such as material processing, spectroscopy, and metrology, to name a few. Material processing with ultrafast pulses has superb aspects such as minimal collateral damage and high precision with the downsides being slow process speed and the requirement of complex laser systems [1]. The ablation-cooled laser material regime demonstrated recently [2] opened the door to transcending the limited ablation rates and the need for tens to hundreds of microjoules which have been impairing ultrafast laser material processing for industrial usage. In this regime, the repetition rate has to be high enough so that there is insufficient time for the targeted spot size to cool down substantially by heat conduction into the rest (bulk) of the target material by the time the next pulse arrives. As a result, the individual pulse energy ablation threshold is scaled down by several orders of magnitude if the repetition rate is simultaneously increased, while the thermal effects to the bulk of the target are also reduced. Furthermore, the simultaneous reduction of pulse energy and the pulse-to-pulse spacing reduces the plasma shielding effects. This is a breakthrough which opens the door to the simplification of ultrafast lasers built for material processing and, hence, boosts the usage of ultrafast fiber lasers outside the laboratory and, consequently, the proliferation of such lasers.

Among the many applications, laser surgery is a promising area for ultrafast laser ablation because it can enable precise cutting with minimal collateral damage and improved after-operation healing process [3]. One can foresee that, with laser systems operating around 2 μm, the ablation cooling regime will take its effect on water-rich soft tissues since laser-tissue interaction is strongly enhanced due to the local peak of water absorption at 1.94 μm. The absorption depth of laser light in liquid water, where 90% of the incident power is absorbed, drops drastically from about 60 mm at a 1 μm wavelength (absorption coefficient ∼0.37 cm^{-1}; it should be emphasized that at this wavelength scattering dominates over absorption) to around 0.2 mm for a 1.94 μm wavelength (absorption coefficient ∼114 cm^{-1}) [4]. Specifically, thulium (Tm)-doped laser systems, which can operate in the vicinity of 1.94 μm, hold a great potential and should be investigated for ablation-cooled laser material removal on soft tissues, in addition to their use in atmospheric sensing, spectroscopy, and processing of polymers [5,6]. In order to carry out such an investigation, ultrafast laser systems with very high repetition rates need to be developed;

burst-mode operation is an ideal tool for obtaining energetic pulses at such repetition rates and practical power levels [7]. In this mode of operation, groups of very high-repetition-rate pulses, called bursts, are repeated at much lower repetition rates, producing reasonable power levels due to the small duty cycles.

In order to study the laser material interactions at high repetition rates, we previously developed the first generation of burst-mode fiber lasers operating at 1 μm [8], improved the uniformity of pulses with electronic feedback [9], and scaled the burst repetition rates to 1 MHz and 100 W for high-power applications [10]. We further investigated the limits of pulse-pumped and continuously pumped burst-mode laser systems by characterizing amplified spontaneous emission (ASE) and achieved 40 μJ pulses in the pulse-pumped and 145 W average power in the continuously pumped systems [11,12]. To better match the requirements of ablation-cooled laser material removal, we reached an in-burst repetition rate of 3.5 GHz by using a repetition rate multiplier after the seed oscillator[13]. In the meantime, Limpert *et al.* demonstrated an impressively high-energy (58 mJ) rod-fiber type burst-mode amplifier [14], further opening new possibilities in burst-mode laser technology. However, all of these fiber burst-mode systems have been built to operate at 1 μm. Up to date, to the best of our knowledge, there has been only one fiber system producing bursts of nanosecond pulses from an electro-optically modulated cavity with a pulse repetition rate of 9 MHz near a 2 μm wavelength [15], but no ultrafast laser systems. Here, we report for the first time, to the best of our knowledge, an ultrafast all-fiber Tm-doped burst-mode laser system with a gigahertz intra-burst repetition rate operating at 2 μm. The laser amplifier system is seeded by a harmonically mode-locked dispersion-managed oscillator operating at a ∼1 GHz repetition rate and is able to produce 500-pulse bursts at a repetition rate of 50 kHz and an average output power of 1 W. The duration of the 40 nJ pulses at the output of the system is around 340 fs which is made possible by the overall dispersion-managed architecture.

The Tm-fiber laser system (Fig. 1) consists of an all-fiber dispersion-managed oscillator, followed by three stages of amplification and a fiber-coupled acousto-optic modulator (AOM) located before the final amplifier which imposes the burst mode on the pulse train. Inside the all-fiber oscillator cavity (Fig. 1), an in-line polarization beam splitter located between two polarization controllers facilitates the nonlinear polarization evolution (NPE) mechanism for mode locking. A home-built erbium-doped fiber amplifier centered at 1560 nm is used to pump 14 cm of highly doped Tm gain fiber (Tm 5/125, Nufern), which is preferred to obtain a high repetition rate. The passive fiber sections of the cavity contain 130 cm of SMF28 and 43 cm of UHNA4 which, together with the 14 cm long Tm fiber, result in a fundamental repetition rate of 107 MHz. With the presence of 43 cm of positive dispersion fiber, UHNA4 ($\beta_2 = 93$ fs^2/mm), a dispersion-managed design is realized, the design of which is guided by pulse propagation simulations for the oscillator cavity [Fig. 2(a)] based on the model described in [16]. The simulation results shown in Fig. 2(a) indicate a significant variation of five-fold for the pulse duration, from 150 fs to 750 fs, and for the spectrum width, from 14 to 21 nm. Overall, the oscillator cavity is dominated by the negative dispersion of 130 cm of SMF28 ($\beta_2 = -71$ fs^2/mm) which, together with UHNA4 and Tm 5/125 ($\beta_2 = -59$ fs^2/mm), yield a net cavity dispersion of −0.062 ps^2.

The oscillator is readily mode-locked at the fundamental repetition rate of 107.6 MHz for a pump power of 470 mW. At this repetition rate, signal power from the 30% output coupler is 25 mW. Harmonic mode-locked states are achieved by increasing the pump level and adjusting the polarization controllers. The limit to the repetition rate is determined by the pump power handling capacity of the Tm fiber, as thermal damage starts to occur above ∼1.3 W of pump power. A stable operation is obtained at the ninth harmonic, 970 MHz [Fig. 3(a)], with a pump power of 1.05 W, where the output from the 30% coupler increases to 170 mW. The long-term stability of the high-harmonic state is quite good and comparable to Yb-doped all-normal dispersion oscillators in the fundamental mode. However, the overall mode-locking stability is highly dependent on the pump wavelength, where no mode locking could be observed for 1555 nm or below, a probable consequence of the very short length of the gain fiber, since absorption in Tm-silica fibers increases towards 1600 nm [17,18]. Compared to previously reported high-repetition-rate Tm fiber lasers [19–21], our oscillator is also the first gigahertz cavity that has an all-fiber architecture with no external saturable absorber components. The overall negative dispersion of the cavity is evidenced by the Kelly sidebands in the 13.5 nm wide spectrum measured at the output [Fig. 3(b)]. Figure 3(c) shows a measured radio-frequency (RF) spectrum with a

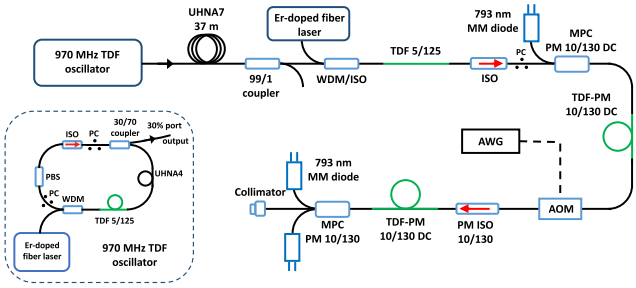

Fig. 1. Schematic diagram of the Tm-fiber burst-mode laser system. TDF, thulium-doped fiber; WDM, wavelength division multiplexer; MM, multimode; ISO, isolator; MPC, multimode pump-signal combiner; DC, double-clad; PM, polarization-maintaining; AOM, acousto-optic modulator; AWG, arbitrary waveform generator; PC, polarization controller; PBS, polarizing beam splitters.

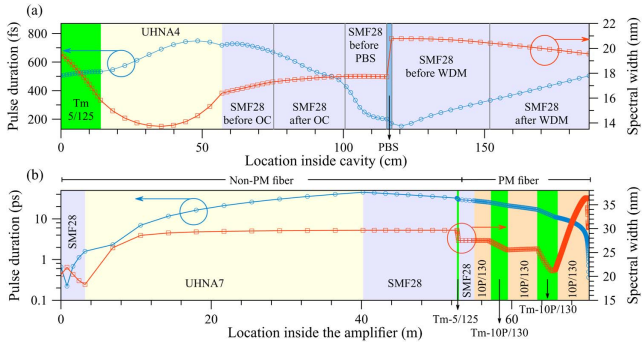

Fig. 2. (a) Simulated pulse duration and spectral evolution along the oscillator cavity. (b) Simulated pulse duration and spectral evolution along an amplifier system following the oscillator output.

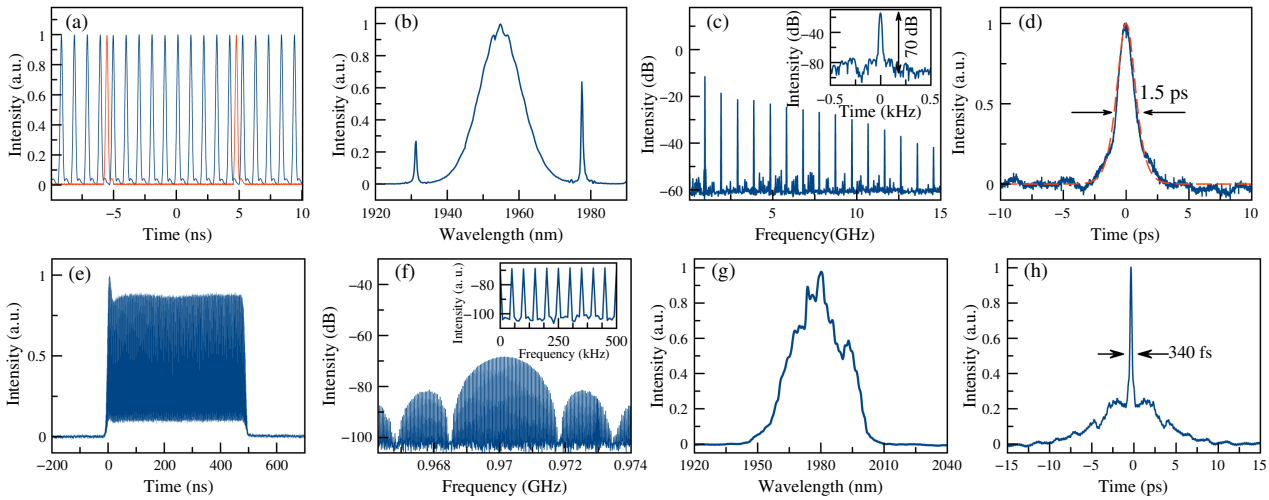

Fig. 3. Oscillator characterization: (a) pulse train for 970 MHz and fundamental repetition frequency of 107.6 MHz (red lines). (b) Optical spectrum from the output port measured after a 3.5 m negative dispersion fiber, (c) RF spectrum of the gigahertz pulse train with a 15 GHz span and 100 kHz resolution. Inset: RF spectrum with a 1 kHz span and 20 Hz resolution bandwidth, with a central frequency of 970 MHz shifted to zero for clarity. (d) Intensity autocorrelation (solid line) of the pulses measured at the same location as the spectrum in (b). Hyperbolic secant square fit (dotted line) to the autocorrelation curve. Amplifier characterization: (e) measured output pulse train for the amplified 500 ns long bursts. (f) RF spectrum with an 8 MHz span and a 1 kHz red resolution bandwidth. Inset: closeup of the RF spectrum showing the comb lines corresponding to the burst repetition frequency of 50 kHz. (g) Optical spectrum of the amplified output. (h) Measured autocorrelation of 40 nJ pulses inside amplified bursts.

15 GHz span and 100 kHz resolution. The super-mode suppression ratio was measured to be ~40 dB. A close-up of an RF spectrum centered at 970 MHz, with a 1 kHz span and a 20-Hz resolution bandwidth, further indicates nearly 70 dB sideband suppression [inset of Fig. 3(c)]. The pulse duration was measured to be 1.5 ps [Fig. 3(d)] after traversing a 3.5 m long negative dispersion fiber section consisting of mainly SMF28, which agrees closely with the simulation result and verifies the accuracy of our simulations. The close fit of the hyperbolic secant-square function [dotted line in Fig. 3(d)] to the autocorrelation curve reinstates the soliton-like characteristics of the pulses generated by the negative dispersion cavity.

The oscillator is followed by the pulse stretcher, where 1.5 ps long pulses are stretched to about ~40 ps by 37 m of positive dispersion fiber, UHNA7 ($\beta_2 = 90$ fs^2/mm), which was preferred for its negative third-order dispersion ($\beta_3 = -33$ fs^3/mm). At 970 MHz, the signal power of 170 mW drops to nearly 117 mW, mainly due to the splice loss between the SMF28 (8.2 μm core diameter) and the UHNA7 (2.4 μm core diameter) fibers. Next, the pulses are amplified up to an average power of 505 mW in a single-mode core-pumped preamplifier built of 20 cm long Tm fiber (5 μm core, 125 μm cladding diameters) pumped by a home-built Er-fiber laser operating at 1560 nm, where its 905 mW of pump power indicates a pump-to-signal conversion efficiency of 43%. Cascading the first preamplifier, the second preamplifier boosts the signal to nearly 3 W, after it is decreased to 270 mW due to losses of 20% and 40% from the isolator and pump-signal combiner, respectively. The second preamplifier composes 2.5 m long double-clad (DC) polarization-maintaining (PM) Tm-doped fiber (10P/130-DC, Nufern) pumped by a 30 W multimode diode at 793 nm through a multimode pump signal combiner (MPC). The pump power is 11.5 W and a 25% conversion efficiency is obtained. Next, the signal is converted into burst mode via an AOM, which has a transmission efficiency of 50%. The burst pattern is electronically fed to the AOM driver by an arbitrary waveform generator (AWG). For 500 ns long bursts repeated at 50 kHz, yielding a 2.5% duty cycle, the signal decreases to less than 40 mW and further to half of this level after the PM isolator, which polarizes the signal. Finally, a backward-pumped DC amplifier containing 3 m of PM Tm-doped fiber (10P/130-DC Nufern) boosts the signal to 1 W average power, yielding 20 μJ burst energy and 40 nJ pulse energy. The conversion efficiency of the final stage, where a 793 nm pump operates at 11.5 W, is rather low, below 10%, due to reduced signal power.

The amplified bursts display a regular pulse train, both regarding individual pulse energy and pulse separation in time [Fig. 3(e)] due to continuous pumping, which reduces gain depletion, ensuring uniformity and harmonic mode locking, respectively. Figure 3(f) shows the measured RF spectrum at 1 W output power with a 8 MHz span and 1 kHz resolution, where the 3 dB bandwidth of 2 MHz for the central lobe corresponds to the 500 ns burst duration. It should also be noted that in spite of the low burst repetition rate, the ASE content in the amplified output should be negligible considering the power level [12] and the long radiative lifetime of the upper laser level (4–6 ms for Tm-silica fibers [18]), which is critical for ASE generation.

The amplified optical spectrum at the output with a bandwidth in the range of 25–30 nm [Fig. 3(g)], about twice as wide as the spectrum of the oscillator, shows that the gain filtering effect is overcome by nonlinear pulse shaping. This is expected since the homogeneously broadened gain bandwidth of Tm-silica fibers covers more than 400 nm [17,18]. Sub-picosecond pulse duration is obtained at the output directly for 40 nJ pulses as a result of the dispersion-management scheme used in the amplifier system. The simulation results in Fig. 2(b) show

the evolution of the pulse width and the spectral width throughout the amplifier system. Note that, according to the simulation, the spectral broadening observed at the output takes place mainly in the final passive fiber section of the amplifier, where the combiner and collimator fibers are located. This is also expected due to the nonlinearity from the amplified pulses being the strongest since the pulses are compressing in time in this section. The length of the UHNA7 stretch fiber was adjusted carefully to optimize the pulse width. The measured autocorrelation in Fig. 3(h) indicates a full width at half-maximum pulse width of 340 fs, when a Gaussian deconvolution factor is used, since the pulse form is expected to transform into dissipative soliton form after the positive dispersion stretch fiber. The pedestal structure observed in the autocorrelation is most likely a consequence of polarization mode beating caused by the unpolarized beam going through birefringent components such as the PM DC fibers and the AOM before it is finally polarized by the isolator after the AOM. The pulse form can be improved in the future conditional upon the availability of a PM isolator for placement between the two preamplifiers.

In conclusion, we have demonstrated the first all-fiber-integrated ultrafast Tm burst-mode amplifier system operating near 2 μm. The intra-burst repetition of 1 GHz is directly generated by the seed oscillator. The dispersion-managed oscillator with a fundamental repetition rate of 107 MHz operates at the ninth harmonic with a high level of stability. The all-fiber amplifier system produces 500-pulse bursts of 20 μJ energy at a repetition rate of 50 kHz. At the output, the 40 nJ pulses inside the bursts have a duration of 340 fs achieved by dispersion management of the overall system with no external compression. This system has been developed to pave the way for the investigation of ablation-cooled laser material removal regime on tissues with high water content, since water has a local absorption peak near 1.95 μm.

Funding. H2020 European Research Council (ERC) (ERC–617521 NLL); TUBITAK (115F098).

REFERENCES

1. K. Sugioka and Y. Cheng, Light Sci. Appl. **3**, e149 (2014).
2. C. Kerse, H. Kalaycıoğlu, P. Elahi, B. Çetin, D. K. Kesim, Ö. Akçaalan, S. Yavaş, M. D. Aşık, B. Öktem, H. Hoogland, R. Holzwarth, and F. Ö. Ilday, Nature **537**, 84 (2016).
3. S. H. Chung and E. Mazur, J. Biophoton. **2**, 557 (2009).
4. J. A. Curcio and C. C. Petty, J. Opt. Soc. Am. A **41**, 302 (1951).
5. K. Scholle, S. Lamrini, P. Koopmann, and P. Fuhrberg, *Frontiers in Guided Wave Optics and Optoelectronics* (Intech, 2010).
6. J. Geng, Q. Wang, and S. Jiang, Proc. SPIE **8164**, 816409 (2011).
7. M. Lapczyna, K. Chen, P. Herman, H. Tan, and R. Marjoribanks, Appl. Phys. A **69**, S883 (1999).
8. H. Kalaycioglu, K. Eken, and F. Ö. Ilday, Opt. Lett. **36**, 3383 (2011).
9. H. Kalaycıoğlu, Y. Eldeniz, Ö. Akçaalan, S. Yavaş, K. Gürel, M. Efe, and F. Ö. Ilday, Opt. Lett. **37**, 2586 (2012).
10. P. Elahi, S. Yılmaz, Y. Eldeniz, and F. Ilday, Opt. Lett. **39**, 236 (2014).
11. H. Kalaycıoğlu, Ö. Akçaalan, S. Yavaş, Y. Eldeniz, and F. Ö. Ilday, J. Opt. Soc. Am. B **32**, 900 (2015).
12. S. Yılmaz, P. Elahi, H. Kalaycıoğlu, and F. Ö. Ilday, J. Opt. Soc. Am. B **32**, 2462 (2015).
13. C. Kerse, H. Kalaycıoğlu, P. Elahi, Ö. Akçaalan, and F. Ö. Ilday, Opt. Commun. **366**, 404 (2016).
14. S. Breitkopf, A. Klenke, T. Gottschall, H.-J. Otto, C. Jauregui, J. Limpert, and A. Tunnermann, Opt. Lett. **37**, 5169 (2012).
15. X. Wang, P. Zhou, X. Wang, H. Xiao, and Z. Liu, Photon. Res. **2**, 172 (2014).
16. B. Öktem, C. Ülgüdür, and F. Ö. Ilday, Nat. Photonics **4**, 307 (2010).
17. S. D. Jackson and T. A. King, J. Lightwave Technol. **17**, 948 (1999).
18. P. Peterka, B. Faure, W. Blanc, M. Karasek, and B. Dussardier, Opt. Quantum Electron. **36**, 201 (2004).
19. Q. Wang, J. Geng, T. Luo, and S. Jiang, Proc. SPIE **8237**, 82371N (2012).
20. C. Bao and C. Yang, Opt. Commun. **356**, 463 (2015).
21. J. Qingsong, W. Tianshu, M. Wanzhuo, W. Zhen, S. Qingchao, B. Baoxue, and J. Huilin, IEEE Photon. J. **9**, 1 (2017).